arXiv:1212.5043v1 [cond-mat.soft] 20 Dec 2012

On shape and electrostatics: competing anisotropies in charged colloidal platelets

Sara Jabbari-Farouji and Emmanuel Trizac
LPTMS, CNRS and Université Paris-Sud, UMR 8626, Bât. 100, 91405 Orsay, France

Jean-Jacques Weis
LPT, CNRS and Université Paris-Sud, UMR 8627, Bât 210, 91405 Orsay, France

Patrick Davidson
Laboratoire de Physique des Solides, CNRS and Université Paris-Sud, UMR 8502 Bât 510, 91405 Orsay, France

Pierre Levitz
Laboratoire PECSA, UMR 7195, Université Pierre et Marie Curie,
Case Courrier 51, 4 place Jussieu, 72522 Paris Cedex 5, France

(Dated: December 21, 2012)

Charged platelet suspensions, such as swelling clays [1–3], disc-like mineral crystallites [4, 5] or exfoliated nanosheets [6, 7], are ubiquitous in nature. Their puzzling phase behaviours are nevertheless still poorly understood: while Laponite and Bentonite clay suspensions [1, 2] form arrested states at low densities, others, like Beidellite and Gibbsite [3, 4], exhibit an equilibrium isotropic-nematic transition at moderate densities. These observations raise fundamental questions about the influence of electrostatic interactions on the isotropic-nematic transition and more generally on the organisation of charged platelets. Here, we investigate the competition between anisotropic excluded-volume and electrostatic interactions in suspensions of thin charged disks, by means of Monte-Carlo simulations. We show that the original intrinsic anisotropy of the electrostatic potential between charged platelets, obtained within the non-linear Poisson-Boltzmann formalism, not only captures the generic features of the complex phase diagram of charged colloidal platelets, but also predicts the existence of novel structures and arrested states upon varying density and ionic strength.

Colloidal suspensions of spherical particles have played a historical role as model systems to elucidate a variety of fundamental phenomena such as glass transition and crystal nucleation [8, 9]. However, many naturally occurring colloids such as tobacco mosaic viruses, DNA strands, swelling clays, and other mineral crystallites are anisotropic. Recent breakthroughs in the synthesis of particles with precisely controlled shapes and interactions have sparked renewed interest in understanding the influence of particle anisotropy on phase behaviour [10, 11], which is required to achieve well-controlled self-assembly and design of novel structures. In the simplest case of axially symmetric particles, anisotropic excluded-volume interactions lead to formation of liquid-crystalline phases [12] while more complex shapes result in remarkable structural diversity [11]. Directional interactions between particles, induced by their geometry and chemical structure, can also lead to anisotropic complex self-assembled structures. When both particle geometry and interactions are anisotropic, the interplay, and even competition between the excluded-volume and other (e.g. electrostatic) interactions may lead to the emergence of novel structures and geometrical frustration. Charged platelet and nanosheet suspensions, that have been widely studied experimentally and that exhibit an intriguing phase behaviour, provide such examples and are the subject matter of this report. For hard-core repulsions only, upon increasing platelet density, a sequence of isotropic, nematic, columnar, and crystalline phases appears, depending on the aspect ratio [13, 14]. Despite several previous studies [15–19], the influence of electrostatic interactions on phase behaviour is still poorly understood and a matter of debate. Previous simulation studies of charged disks suffer from not taking into account the renormalised effective charge and the full orientational dependence of interactions. Furthermore, most of them are based on coarse-grained interaction site models [16–18], which is computationally costly. Here, such shortcomings are circumvented: our approach is based on a well controlled effective electrostatic potential between two disks, that depends on their relative distance and orientation. We shall neglect van der Waals interactions, size and charge polydispersity to focus on repulsive electrostatic interactions that we deem most relevant. We address two important questions: i) how do electrostatic interactions influence the isotropic-nematic (I/N) transition? ii) can the experimentally-observed arrested states occur within our model and what are their natures?

We account for electrostatic interactions between charged disks, in an electrolyte medium with inverse Debye length κ, at the two-body level using Poisson-Boltzmann formalism [20, 21]. The far-field potential for two charged disks with diameter σ, centres at a distance r apart, and with normals making angles θ_i with the centre-to-centre line, reads:

$$\frac{U_{12}(r/\sigma,\theta_1,\theta_2)}{k_BT} = \lambda_B Z_{eff}^2(\kappa\sigma) f(\kappa\sigma,\theta_1) f(\kappa\sigma,\theta_2) \frac{\exp(-\kappa r)}{r}. \tag{1}$$

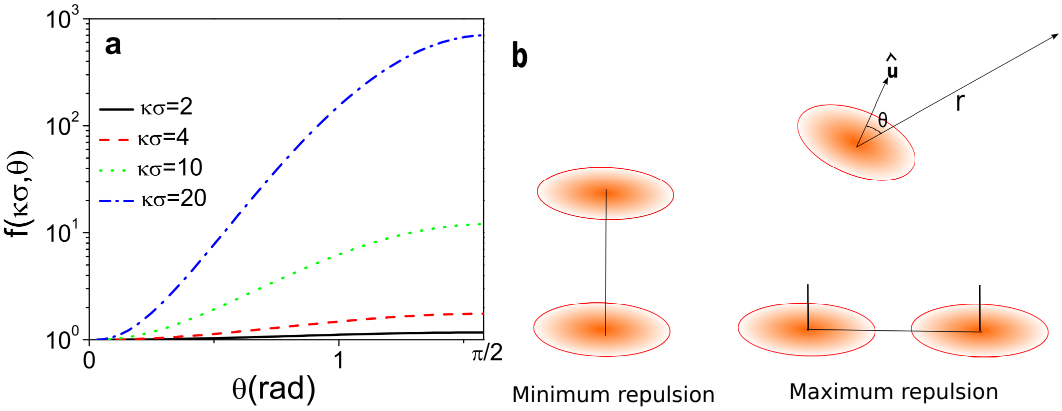

FIG. 1. **Characteristic anisotropy of electrostatic potential of charged disks in an electrolyte.** a) Anisotropy function $f(\kappa\sigma,\theta)$ versus θ, the angle between the disk normal $\widehat{u}$ and the line of observation, for several values of ionic strength $\kappa\sigma$ b) Two interacting parallel charged disks in stacked and coplanar configurations with equal centre to centre distance correspond to minimum and maximum repulsion, respectively.

where Z_{eff} is the effective charge; it depends on the platelet bare charge and the ionic strength through κ. For highly charged platelets as considered here, Z_{eff} saturates to a value $Z_{eff}^{sat}\lambda_B/\sigma = 0.5\kappa\sigma + 1.12$, where λ_B is the Bjerrum length (7.1 Å in water at room temperature). The anisotropy function $f(\kappa\sigma,\theta)$ encodes the orientational dependence of the potential and can be expressed in terms of spheroidal wave functions [21]. $f(\kappa\sigma,\theta)$ increases with angle θ, reaching a maximum in the disc plane ($\theta = \pi/2$) (Fig. 1a). It furthermore is enhanced by the ionic strength: a smaller Debye length acts as a probe which reveals asphericity. This results in a strong asymmetry between coplanar and stacked configurations (Fig. 1b), a notable difference with standard Heisenberg-like models. A competition between the excluded volume and electrostatic effects ensues, which is a generic feature for charged oblate spheroids. This interplay has important consequences on the phase behaviour and allows for the formation of new structures.

We have investigated the structure and dynamics of hard disks interacting by the anisotropic Yukawa potential of Eq. 1 by Monte-Carlo simulations [22]. The degree of orientational order was characterised by the nematic order parameter $S \equiv \langle P_2(\cos(\psi))\rangle = \left\langle \frac{1}{2}(3\cos^2\psi - 1)\right\rangle$ where ψ is the angle of a platelet normal with the director $\widehat{n}$ and the brackets mean averaging over all particles. Hence, $-1/2 < S < 1$ with $S = 0$ for the disordered isotropic phase. When $0 < S < 1$, the platelet normals point on average along the director $\widehat{n}$ while in the more unconventional $S < 0$ regime, the platelet normals are on average perpendicular to $\widehat{n}$ ("antinematic" order). Upon varying density and ionic strength, we found eight distinct structures (Fig. 2). Four of them have a vanishing S and are formed at low and moderate densities. Three of these structures, isotropic fluid, plastic crystal (structure with positional order but no orientational order), and "random stacks", are orientationally disordered while the fourth one is a novel structure that consists of intertwined nematic and anti-nematic layers (Fig. 2). We coin it "nematic-antinematic intergrowth texture". The orientationally ordered phases with $S > 0.4$ which appear at higher densities include two liquid-crystalline phases, i.e. nematic phase of platelet stacks (sometimes called "columnar nematic") and hexagonal columnar phase, together with two crystalline phases with bcc-like and hexagonal symmetry.

Before turning to a comparison with experiments, we present the phase diagram. It is essential to emphasise that our equilibration procedure for $\rho^* = \rho\sigma^3 > 3$ requires a careful and gradual increase of disk charge from zero to the desired value, to ensure attaining configurations close to equilibrium. More rapid quenches generally put the system out of equilibrium, and for high enough densities, we therefore expect discrepancies with the experimentally observed states, that have presumably not reached equilibrium. We now highlight important aspects of the phase diagram (Fig. 3) in connection with the features of our pair potential. A significant hallmark is the non-monotonic behaviour of orientational disorder-order transition with $\kappa\sigma$ which results from the opposing effects of the decreasing potential range and the increasing amplitude of the anisotropy function, upon increasing ionic strength; Z_{eff}^{sat} also increases with ionic strength but we verified that the observed trend is unchanged provided $Z_{eff}\lambda_B/\sigma > 2.3$.

In the limit of low ionic strengths ($\kappa\sigma = 1$), where the potential is rather isotropic and long-ranged, bcc-like structures are formed, as observed with charged spheres at low $\kappa\sigma$ [23]. At low densities, disks are orientationally disordered (plastic crystal) and are reminiscent of Wigner crystals observed for low volume fractions of charged spheres [24]. Increasing the ionic strength, at $\kappa\sigma = 2$ where the amplitude of the anisotropy function is less than 1.2, the plastic crystal is replaced by an isotropic fluid at low and moderate densities. The crystal disappearance for a slightly larger $\kappa\sigma$ and shorter range of potential highlights the geometrical frustrating effect of anisotropy. At $\kappa\sigma = 2$, in the high density regime, the long-range positional order is still preserved as crystals with hexagonal symmetry appear.

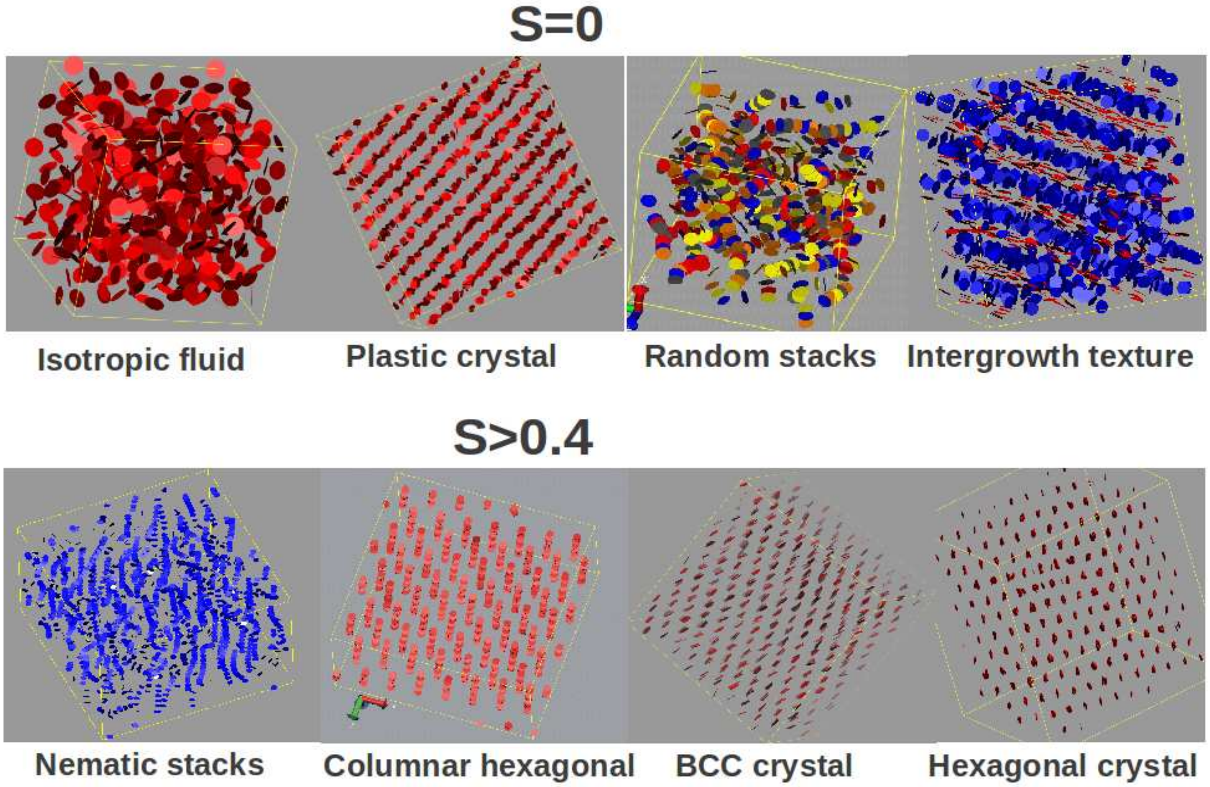

FIG. 2. **Summary of found structures for charged disks.** We recognise eight distinct configurations, four of which have a vanishing orientational order parameter S. These include isotropic fluid, plastic crystal, "random stacks" and a novel "intergrowth texture" that is composed of disks arranged in alternating nematic (red colour) and antinematic (blue colour) layers. The orientationally ordered structures with $S > 0.4$ encompass nematic and columnar hexagonal liquid-crystals in addition to two crystalline phases with bcc and hexagonal symmetry. Note that the disks are not displayed with their real size, but with 20 to 40 % their diameter.

Interestingly, for large enough ionic strengths ($4 \leq \kappa\sigma \leq 6$) and at moderate densities, the new intergrowth texture appears and, for $\kappa\sigma \geq 8$, randomly oriented stacks of disks are observed. The intergrowth texture consists of sets of aligned disks ($0.75 < S < 0.93$) interspersed with layers exhibiting anti-nematic order ($-0.45 < S < -0.3$). Both types of layers share the same director. Here, the particles organise with relative T-shape configurations, intermediate between coplanar and stacked. At still higher densities, further increase of ionic strength ($\kappa\sigma \geq 4$), leads to weakening of the positional order. Hexagonal crystals are replaced by hexagonal columnar liquid-crystals with no positional correlations along the hexagonal axis.

To better characterise the orientationally disordered structures, we examined their translational and rotational dynamics by dynamic Monte-Carlo method [25]. We computed self-intermediate scattering functions $F_s(q,t) = \langle \exp[i\vec{q} \cdot (\vec{r}(t) - \vec{r}(0))] \rangle$ and time orientational correlation functions $\langle P_2(\widehat{u}(t) \cdot \widehat{u}(0)) \rangle$. In the isotropic fluid, both translational and rotational correlation functions decay on a rather fast time scale (Fig. 4), whereas, in the random stacks phase and intergrowth texture, the orientational time correlation functions show very little decay within the longest time-scale probed, in contrast to their translational counterparts. In random stacks, increasing ρ^* from 2 to 3 has a spectacular effect on orientational relaxation (Fig. 4b), which becomes completely hindered; the dynamics of this structure that lacks long-range orientational order, is reminiscent of that in orientational glasses [26]. This state results from the strongly anisotropic and short-ranged character of the potential for sufficiently large $\kappa\sigma$, where the locally favoured stacking leads to frustration and hinders the onset of orientational ordering. On the other hand, the plastic crystals exhibit slow dynamics for translational coordinates and fast decay for orientational ones.

We now compare our simulations against the most extensively studied charged colloidal platelets: Gibbsite, Beidellite, and Laponite systems. Gibbsite and Beidellite show an I/N transition for a wide range of ionic strengths, and platelet stacking is often observed in the nematic phase. Moreover, Gibbsite suspensions also display a columnar hexagonal liquid-crystalline phase. These features are well captured in our simulations. Fig. 5 shows the phase diagrams of Gibbsite [4] and Beidellite [3], drawn versus reduced density ρ^* and $\kappa\sigma$ for quantitative comparison. Overall,

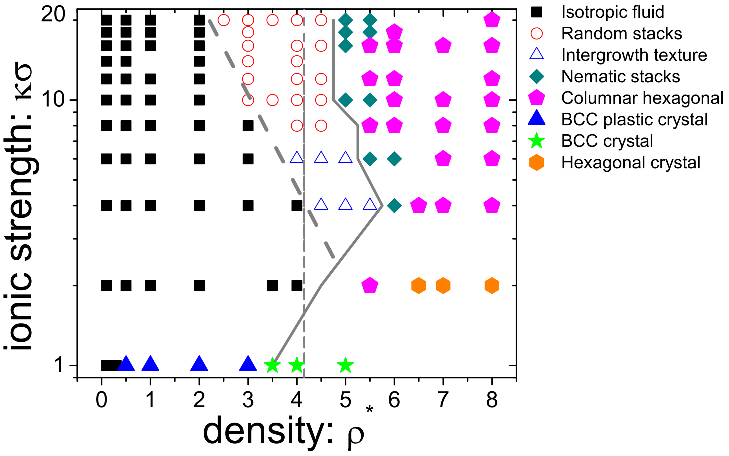

FIG. 3. **Phase diagram of repulsive charged disks** as a function of dimensionless density $\rho^* = \rho\sigma^3$ and ionic strength $\kappa\sigma$. The vertical dashed line shows the density beyond which the nematic phase for hard disks (thus without electrostatic interactions) appears. The solid line separates the orientationally ordered (right hand side) and disordered phases (left hand side). The dashed line is a guide to the eyes to show, on the right hand side, the regions where the structures with slow orientational dynamics appear.

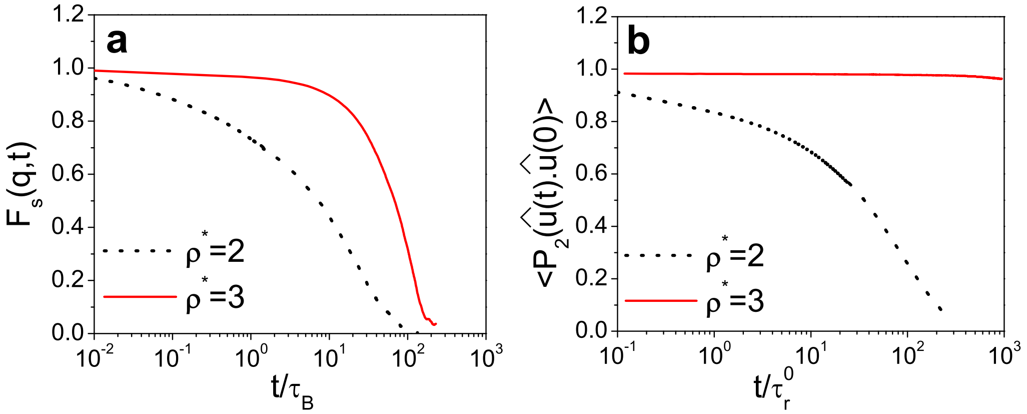

FIG. 4. **Dynamics in isotropic fluid and random stacks structure.** a) Self-intermediate scattering function $F_s(q,t)$ computed at $q\sigma = 7$ and b) orientational time correlation function $\langle P_2(\widehat{u}(t) \cdot \widehat{u}(0))\rangle$ for an anisotropic fluid $\kappa\sigma = 20$, $\rho^* = 2$ and random stacks $\kappa\sigma = 20$, $\rho^* = 3$. The time-scales are expressed in terms of characteristic time of free translational $\tau_B \equiv \sigma^2/(6D_0^t)$ and rotational $\tau_0^r \equiv 1/(2D_0^r)$ diffusions, respectively.

the agreement between our simulations and the experimental phase diagrams for Gibbsite [4] and Beidellite [3] (shown in Fig. 5) is quite remarkable. In both Gibbsite and Beidellite, for $10 < \kappa\sigma < 20$, a nematic phase of stacked platelets is found, although at densities slightly lower than the simulated ones. This small discrepancy could be due to platelet polydispersity that usually widens the isotropic-nematic coexistence region. Furthermore, for Gibbsite particles at lower ionic strengths, a direct transition from isotropic to columnar hexagonal phases is observed, which is again similar to our results at $\kappa\sigma = 8$. Upon further increase of density, a nematic gel is experimentally observed whereas we obtained a columnar hexagonal phase. At such high densities, we already anticipated that the suspensions cannot easily reach equilibrium, since the simulations require a slow and careful procedure to relax. Furthermore, the nematic gel of Gibbsite is a jammed state of oriented stacks (columns) that evolves towards a columnar hexagonal structure with time [27].

In contrast to Gibbsite and Beidellite, the I/N transition in Laponite suspensions is hindered by the occurrence of various kinetically trapped states at very low volume fractions ($\phi < 0.02$) and formation of these states is shifted towards lower densities upon increasing ionic strength [1]. The range of densities and ionic strengths investigated in experiments corresponds to $\rho^* < 1$ and $1 \leq \kappa\sigma < 20$. At such low densities, we observe a solid-like state (plastic crystal) only at small $\kappa\sigma = 1$. This state could presumably only be glassy if polydispersity were considered [28].

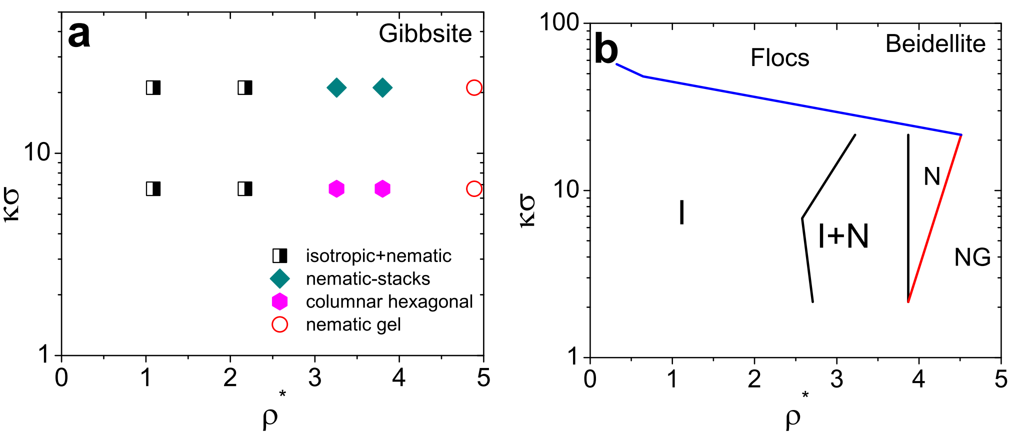

FIG. 5. **Comparison to experiments.** Experimental phase diagrams of a) Gibbsite [4] and b) Beidellite [3]. The phases corresponding to each symbol are indicated in the legend. Here, I refers to isotropic, N to Nematic stacks phase and NG to nematic Gel.

Upon further increase of ionic strength, we observe an ergodic repulsive isotropic liquid in the low-density region of our phase diagram. Interestingly, at somewhat higher densities and for $\kappa\sigma \geq 10$, we find signatures of an orientational glass that is formed at lower densities upon increase of ionic strength, similar to the trend observed for Laponite. Our model system only based on repulsive interactions cannot fully explain the phase behaviour of Laponite for larger ionic strengths; these discrepancies point to the possible relevance of attractive interactions [29]. Nevertheless, our approach hints at the existence of a solid-like state at low ionic strengths, in agreement with the experimental observation of a Wigner glass [30].

In conclusion, numerical simulations of charged platelets, interacting with an effective potential obtained from Poisson-Boltzmann theory, show a rich phase diagram. We thereby capture the generic features of the experimental systems. The required procedure of slow charge increase, at moderate and high densities, echoes the difficulty for experimental systems to reach thermodynamic equilibrium. Better agreement with experiments could be achieved by considering polydispersity, platelet flexibility, and interactions specific to each system such as van der Waals attractions. The features brought to the fore here, though, can be considered as the non-specific effects pertaining to charged colloidal platelets. In particular, the robust form of our screened Coulomb potential leads to the formation of orientational glasses (random stacks and novel intergrowth texture), which calls for further experimental investigations in the isotropic region of the phase diagrams close to the I/N transition.

I. METHODS

We carried out canonical (NVT) Monte-Carlo simulations [22] on a system of N thin hard disks of diameter σ in a cubic simulation box of side L with periodic boundary conditions using the anisotropic two-body potential of Eq. 1. The simulations were performed at $T = 300$ K for a wide range of densities $\rho^* = N\sigma^3/L^3 = 0.1 - 8$ and ionic strengths $\kappa\sigma = 1 - 20$. The diameter σ/λ_B was taken to be 43.1 in the simulations. The number of particles varied between $500 \leq N \leq 10976$, although most of the simulations were performed for $N = 1024$ or $N = 1372$. For ionic strengths $\kappa\sigma \leq 2$, we adopted an Ewald-like scheme to take into account the relatively long range of the potential [31]. Due to the rather large values of the effective charge, we encountered some convergence difficulties for equilibration of large densities, $\rho^* \geq 3$ as the obtained final configuration depended on the initial one. Therefore, we adopted the following procedure: we started from an initial equilibrium configuration of (uncharged) disks at the desired density; then increased the charge gradually to the final value $Z_{eff}^{sat}(\kappa\sigma)$ allowing the system to equilibrate at each step. The required procedure is akin to simulated annealing used in spin glasses.

ACKNOWLEDGMENTS

S. J-F would like to acknowledge the financial support from Foundation Triangle de la Physique and IEF Marie-Curie fellowship. We are also grateful to A. Maggs and H. H. Wensink for fruitful discussions.

Author contributions

S. J-F carried out the simulations, analysed the data, and wrote the manuscript. J-J. W. performed the simulations and analysed the data. P. D. participated in understanding of results and writing of the manuscript. P. L. contributed to the comparison of results with experiments. E. T. initiated and supervised the research. All authors contributed to rationalising

the data.

Additional information

The authors declare no competing financial interests.

---

[1] Ruzicka, B. and Zaccarelli, E. A fresh look at Laponite phase diagram. *Soft Matter* 7, 1268–1286 (2011).

[2] Gabriel, J.-C. P., Sanchez, C. and Davidson, P. Observation of nematic liquid-crystal textures in aqueous gels of smectite Clays *J. Phys. Chem.* 100, 11139–11143 (1996).

[3] Paineau, E. et al. Liquid-crystalline nematic phase in aqueous suspensions of a disk-shaped natural beidellite clay. *J. Phys. Chem. B* 113, 15858–15869 (2009).

[4] Mourad, M. C. D., Byelov, D. V., Petukhov, A. V., Matthijs de Winter, D. A., Verkleij, A. J. and Lekkerkerker, H. N. W. Sol-gel transitions and liquid crystal phase transitions in concentrated aqueous suspensions of colloidal gibbsite platelets *J. Phys. Chem. B* 113, 11604–11613 (2009).

[5] Sun, D., Sue, H.-J., Cheng, Z., Martnez-Ratn, Y. and Velasco, E. Stable smectic phase in suspensions of polydisperse colloidal platelets with identical thickness *Phys. Rev. E* **80**, 041704 (2009).

[6] Z. Liu , et al. Synthesis, anion exchange, and delamination of Co-Al layered double hydroxide: assembly of the exfoliated nanosheet/polyanion composite films and magneto-optical studies. *J. Am. Chem. Soc.* 128 (14), 4872–4880 (2006)

[7] Yamaguchi, D., et al. Aspect-ratio-dependent phase transitions and concentration fluctuations in aqueous colloidal dispersions of charged platelike particles. *Phys. Rev. E* 85, 011403 (2012).

[8] Pusey, P. N. and van Megen, W. Phase behaviour of concentrated suspensions of nearly hard spheres, *Nature* 320, 340–342 (1986).

[9] Gasser, U., Weeks, E. R., Schofield, A., Pusey, P.N. and Weitz, D. A. Real-space imaging of nucleation and growth in colloidal crystallization. *Science* 292, 258262 (2001).

[10] Glotzer, S. C. and Solomon, M. J. Anisotropy of building blocks and their assembly into complex structures. *Nature materials* 6, 557–562 (2007).

[11] Damasceno, P. F., Engel, M., Glotzer, S. C. Predictive Self-Assembly of Polyhedra into Complex Structures. *Science* **337**, 453–457 (2012).

[12] Onsager, L. The effects of shape on the interaction of colloidal particles.*Ann. N. Y. Acad. Sci.* 51, 627–659 (1949).

[13] Veerman, J. A. C. and Frenkel, D. Phase behavior of disklike hard-core mesogens. *Phys. Rev. A* 45, 5632–5648 (1992).

[14] Marechal, M., Cuetos, A., Martinez-Haya, B., and Dijkstra, M. Phase behavior of hard colloidal platelets using free energy calculations *J. Chem. Phys.* **134**, 094501 (2011).

[15] M. Dijkstra, J. P. Hansen and P. A. Madden, Gelation of a clay colloid suspension. *Phys. Rev. Lett.* 75, 2236–2239 (1995).

[16] Kutter, S., Hansen, J., Sprik, M. and Boek, E. Structure and phase behavior of a model clay dispersion: A molecular-dynamics investigation. *J. Chem. Phys.* 112, 311–323 (2000).

[17] Mossa, S., de Michele, C. and Sciortino, F. Aging in a Laponite colloidal suspension: A Brownian dynamics simulation study. *J. Chem. Phys.* 126, 014905 (2007).

[18] Delhorme, M., Jönsson, B. and Labbez, C. Monte Carlo simulations of a clay inspired model suspension: the role of rim charge *Soft Matter.* 8, 9691–9704 (2012).

[19] Morales-Anda, L., Wensink, H. H., Galindo, A. and Gil-Villegas, A. Anomalous columnar order of charged colloidal platelets *J. Chem. Phys. 132*, 034901 (2012).

[20] Agra, R., Trizac, E., and Bocquet, L. The interplay between screening properties and colloid anisotropy: Towards a reliable pair potential for disc-like charged particles. *Eur. Phys. J. E* 15, 345–357 (2004).

[21] Álvarez, C. and Téllez, G. Screening of charged spheroidal colloidal particles *J. Chem. Phys.* 133, 144908 (2010).

[22] M. P. Allen and D. J. Tildesley, *Computer Simulation of Liquids* (Oxford University Press, Oxford, 1987).

[23] Hynninen, A-P. and Dijkstra, M. Phase diagrams of hard-core repulsive Yukawa particles. *Phys. Rev. E* 68, 021407 (2003).

[24] Lindsay, H. M. and Chaikin, P. M. Elastic properties of colloidal crystals and glasses. *J. Chem. Phys.* 76, 3774–3782 (1982).

[25] Jabbari-Farouji, S. and Trizac, E. Dynamic Monte Carlo simulations of anisotropic colloids. *J. Chem. Phys.* 137, 054107 (2012).

[26] Zheng, Z., Wang, F. and Han, Y. Glass Transitions in Quasi-Two-Dimensional Suspensions of Colloidal Ellipsoids. *Phys. Rev. Lett.* 107, 065702 (2011).

[27] Mourad, M. C. D., Byelov, D. V., Petukhov, A. V. and Lekkerkerker, H. N. W. Structure of the repulsive gel/glass in suspensions of charged colloidal platelets. *J. Phys. Condens. Matter* 20, 494201 (2008).

[28] Zaccarelli, E., Andreev, S., Sciortino, F. and Reichman, D. R. Numerical Investigation of Glassy Dynamics in Low-Density Systems. *Phys. Rev. Lett.* 100, 195701 (2008).

[29] Ruzicka, B., Zaccarelli, E., Zulian, L., Angelini, R., Sztucki, M., Moussaid, A., Narayanan, T. and Sciortino, F. Observation of empty liquids and equilibrium gels in a colloidal clay. *Nature Materials* 10, 56 (2011).

[30] Levitz, P., Lecolier, E., Mourchid, A., Delville, A. and Lyonnard, S. Liquid-solid transition of Laponite suspensions at very low ionic strength: Long-range electrostatic stabilisation of anisotropic colloids. *Europhys. Lett.* **49**, 672–677 (2000).

[31] Salin G. and Caillol, J.M. Ewald sums for Yukawa potentials. *J. Chem. Phys.* **113**, 10459–10463 (2000).